catalysts

MDPI

Article

Ternary Composite of Co-Doped CdSe@electrospun Carbon Nanofibers: A Novel Reusable Visible Light-Driven Photocatalyst with Enhanced Performance

Gopal Panthi [1], Oh Hoon Kwon [2], Yun-Su Kuk [3], Kapil Raj Gyawali [4], Yong Wan Park [2] and Mira Park [1,*]

1 Department of Biomedical Sciences and Institute for Medical Science, Jeonbuk National University, Jeonju 54907, Korea; gopalpanthi2003@gmail.com
2 Research and Development Division, Korea Institute of Convergence Textile, Iksan 54588, Korea; simulation@kictex.re.kr (O.H.K.); pywspirit@kictex.re.kr (Y.W.P.)
3 Korea Institute of Carbon Convergence Technology (KCTECH), Jeonju 54853, Korea; yunsu@kctech.re.kr
4 Department of Chemistry, Birendra Multiple Campus, Tribhuvan University, Bharatpur 442000, Chitwan, Nepal; kapgyawali10@gmail.com
* Correspondence: wonderfulmira@jbnu.ac.kr; Tel.: +82 63 2703105

Received: 21 February 2020; Accepted: 18 March 2020; Published: 20 March 2020

Abstract: In this work, flexible ternary composites of cobalt-doped cadmium selenide/electrospun carbon nanofibers (Co-CdSe@ECNFs) for photocatalytic applications were fabricated successfully via electrospinning, followed by carbonization. For the fabrication of the proposed photocatalysts, Co-CdSe nanoparticles were grown in situ on the surface of ECNFs during the carbonization of precursor electrospun nanofibers obtained by dispersing Se powder in the electrospinning solution of polyacrylonitrile/*N*,*N*-Dimethylformamide (PAN/DMF) containing Cd^{2+} and Co^{2+}. The photocatalytic performance of synthesized samples is investigated in the photodegradation of methylene blue (MB) and rhodamine B (RhB) dyes. Experimental results revealed the superior photocatalytic efficiency of Co-CdSe@ECNFs over undoped samples (CdSe@ECNFs) due to the doping effect of cobalt, which is able to capture the photogenerated electrons to prevent electron–hole recombination, thereby improving photocatalytic performance. Moreover, ECNFs could play an important role in enhancing electron transfer and optical absorption of the photocatalyst. This type of fabrication strategy may be a new avenue for the synthesis of other ECNF-based ternary composites.

Keywords: electrospinning; carbon nanofibers; ternary composite; CdSe; photocatalyst; visible light

1. Introduction

Contamination of bodies of water such as ground water, lakes, rivers, and seas with toxic chemicals or foreign substances caused by improper disposal of waste water from different industrial plants has become a global challenge, as these contaminants have adverse effects on human and aquatic life. However, while industrialization is the key initiator of development and urbanization of a society, it has been recognized as a major cause of water pollution. The effluents discharged from industrial plants contain a number of toxic pollutants ranging from organochloride-based pesticides to heavy-metal-associated non-biodegradable organic dyes, which cause the contamination of natural water sources and subsequent health problems [1]. Different attempts, comprising biological treatment, adsorption by activated carbon, reverse osmosis, coagulation, and ion exchange, have been made to address the issue of water contamination, however, none of these conventional water treatment

techniques are capable of eliminating the pollutants completely and require further treatment, making the whole process more costly [2,3]. Therefore, there is significant demand to develop new techniques which efficiently and economically reduce organic pollutants present in industrial waste water. In this regard, photocatalysis, a green technique, has emerged as a novel, simple, cost-effective, and potential remedy for the elimination of a wide range of organic pollutants [4]. Depending on the phenomenon of initial photoexcitation, the photocatalysis process has been divided into two categories. The process in which initial photoexcitation occurs in the photocatalyst and the photoexcited electrons get transferred into ground-state molecules (e.g., dye molecules) is referred to as the catalyzed photoreaction process. On the other hand, if the initial photoexcitation occurs in adsorbent molecules (e.g., dye molecules) and the photoexcited electrons interact with the ground-state photocatalyst, the process is referred to as sensitized photoreaction [5]. In practical application, the principle of catalyzed photoreaction can be implemented in the photodegradation of organic pollutants present in waste water using semiconductor materials [6,7]. Similarly, dye-sensitized solar cells that can convert solar energy into a usable form can be manufactured by applying the principle of sensitized photoreaction, in which dye molecules can play an important role for broader and more intense absorption of light [8]. The discovery of the electrochemical photocatalysis of water at a TiO_2 electrode by Honda and Fujishima in 1972 opened a new door for designing and fabricating semiconductor-based photocatalysts such as metal oxides, metal sulfides, and composite materials to be applied in photocatalytic applications [9–13]. To date, various composite materials have been investigated for their photocatalytic application [14–17]. More specifically, intense research interest has been drawn towards the fabrication of visible-light-driven photocatalysts which can potentially utilize solar energy (a renewable energy source) to create a comfortable environment for all living beings [18,19].

Among various semiconductor materials, CdSe (a II-IV semiconductor material) has drawn significant attention towards photocatalytic application due to its low band gap energy (1.75 eV) and high light-responding ability [20]. However, its practical applications are limited due to low surface adsorptive ability, low dispersity, and high recombination rate of photogenerated electrons and holes [21,22]. To overcome the aforementioned limitations of CdSe, a number of research works have been carried out, which have been mainly focused on synthesis strategy, either by coupling with other semiconductor materials or by forming composites to keep or enhance the performance of the solar light harvesting photocatalyst [20,22–24]. Additionally, a large number of reports regarding the enhancement of photocatalytic performance of semiconductor photocatalysts doped with transition metal ions have been published. Semiconductor photocatalysts doped with transition metal ions significantly influence the photoreactivity by changing the recombination rates of electron–hole pairs and interfacial electron transfer due to the electronic synergetic effect between semiconductors and transition metals [25,26]. Furthermore, a dopant ion can enhance the photocatalytic activity of a photocatalyst by prolonging the lifetime of light-induced charge carriers [27,28]. Agglomeration and separation difficulties are the main concerns that arise in the practical application of a photocatalyst when used in powder form [29]. Therefore, carbonaceous materials such as carbon nanotubes [30,31], graphene oxide [32,33], carbon spheres [34,35] and ECNFs [36,37] are being used as support material for photocatalysts to prevent agglomeration and enhance their photocatalytic performance. These carbonaceous materials not only provide a platform to deposit semiconductor photocatalysts, but also accelerate the photogenerated electrons and speed up photocatalytic reactions by reducing electron–hole recombination [31,37].

Therefore, based on the advantages of carbonaceous materials as support and transition metal ions as dopant, our work is focused on the fabrication of a ternary composite of Co-doped CdSe @ electrospun carbon nanofibers (Co-CdSe@ECNFs) in order to investigate its photocatalytic activity towards the photodegradation of organic dyes. Because of their one-dimensional structure, high specific surface area, good electrical conductivity, and high chemical stability, ECNFs are widely used as supports of photocatalyst nanoparticles. The longitudinal conductive length of ECNFs serves as a conductivity network which captures and transfers photogenerated electrons, improving the photocatalytic performance of photocatalysts [36,38]. Following from this, the fabrication of

Co-CdSe@ECNFs might be an ideal strategy to obtain a ternary composite as an efficient photocatalyst. To the best of our knowledge, this type of work has not been reported so far.

2. Results and Discussion

Figure 1 illustrates the X-ray diffraction (XRD) patterns of ECNFs, CdSe@ECNFs, and Co-CdSe@ECNFs. The characteristic peaks displayed by CdSe@ECNFs and Co-CdSe@ECNFs at 2θ of 25.24°, 42.2°, and 49.9° corresponding to the crystallographic planes (111), (220), and (311) were associated with the cubic CdSe phase (JCPDS: 65-2891). The peak displayed by all samples at 2θ of 22.5° was associated with the (002) crystallographic plane of graphitic carbon. However, none of the characteristic peaks of Co and its compound impurity were detected in the XRD pattern of Co-CdSe@ECNFs, which might be attributed to the substitution of Cd^{2+} by Co^{2+} from the CdSe crystal lattice due to the smaller radius of Co^{2+} (0.75 Å) compared to that of Cd^{2+} (0.95 Å). Therefore, Co^{2+} could be easily inserted into the CdSe crystal lattice, rather than forming a mixture [39].

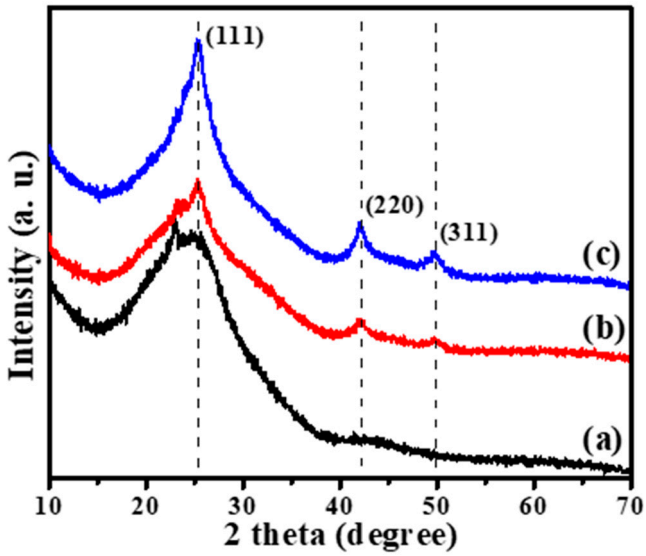

Figure 1. XRD diffraction patterns: (**a**) Electrospun carbon nanofibers (ECNFs), (**b**) Cadmium selenide/electrospun carbon nanofibers (CdSe@ECNFs), and (**c**) Co-doped CdSe@ECNFs (Co-CdSe@ECNFs).

The morphology and elemental composition of different samples are presented in field emission scanning electron microscopy (FESEM) images (Figure 2). Figure 2a shows a typical FESEM image of ECNFs. As can be seen, ECNFs were uniform, continuous, randomly oriented, and possessed smooth surfaces without secondary nanostructures. In comparison with ECNFs, no apparent change was observed in the overall pattern of CdSe@ECNFs (Figure 2b) and Co-CdSe@ECNFs (Figure 2c). However, the surface of the carbon nanofibers was no longer smooth. The high-magnification images (insets of Figure 2b,c) reveal that the surfaces of the ECNFs were coarse due to the growth of numerous nanoparticles after carbonization. The nanoparticles were uniformly distributed across the surface of each carbon nanofiber without aggregation, thereby offering a high surface area for the nanoparticles. Figure 2d represents the energy dispersive X-ray spectroscopy (EDS) spectrum along with wt% of elements (inset) of Co-CdSe@ECNFs. As shown in the spectrum, the existence of considerable amounts of C, Co, Cd, and Se elements could confirm the doping of Co in CdSe nanoparticles supported on ECNFs. The inset in Figure 2a is a digital photograph of a flexible nanofibrous mat of Co-CdSe@ECNFs. Moreover, the elemental mapping images of Co-CdSe@ECNFs (Figure 3) reveal the uniform distribution of Co, Cd, and Se elements on the surface of carbon nanofibers, signifying the successful fabrication of the ternary composite.

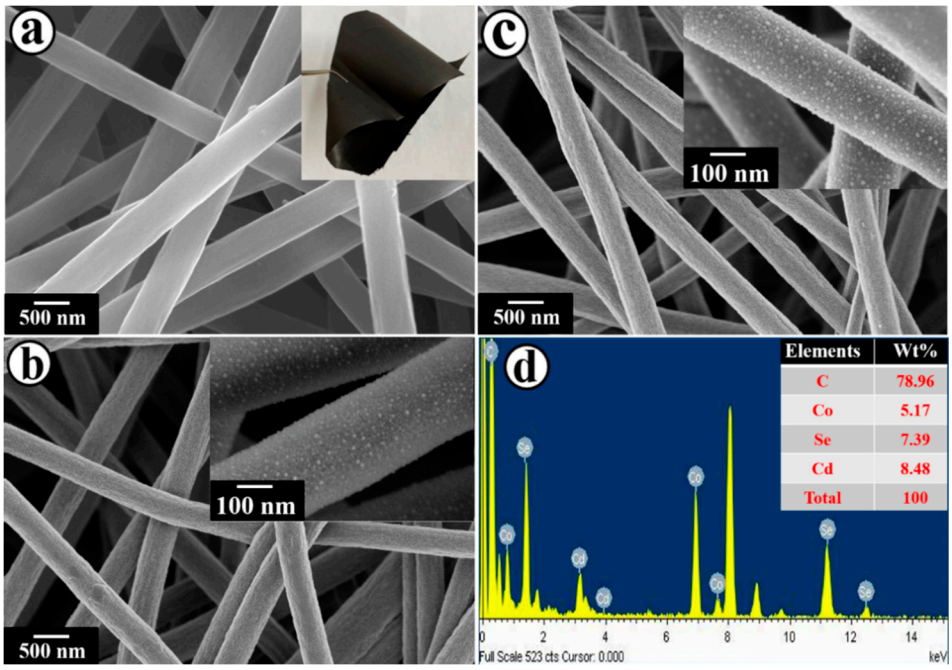

Figure 2. FESEM images: (**a**) ECNFs, (**b**) CdSe@ECNFs, and (**c**) Co-CdSe@ECNFs. Panel (**d**) represents the corresponding EDS of (**b**). Insets: (**a**) digital photograph of Co-CdSe@ECNFs, (**b**,**c**) high-magnification images of corresponding nanofibers, and (**d**) wt% of elements present in Co-CdSe@ECNFs.

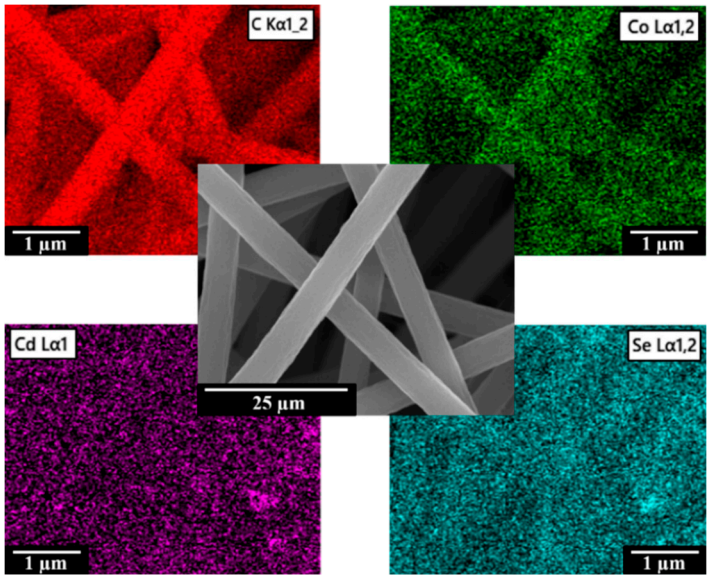

Figure 3. Elemental mapping of Co-CdSe@ECNFs.

In order to observe the fiber morphology and degree of dispersion of nanoparticles on the surface of ECNFs, transmission electron microscopy (TEM) analysis was performed (Figure 4). Figure 4a shows a TEM image of an ECNF with a nanofibrous morphology possessing a relatively smooth surface. In comparison, the surface of Co-CdSe@ECNFs were somewhat rough due to the growth of numerous Co-CdSe nanoparticles on the surface of the ECNFs, as described in the FESEM analysis. The nanoparticles having an average size of 9 nm grew uniformly on the surface of ECNFs, as shown in the high-magnification TEM image (Figure 4c) obtained from the red circled area of Figure 4b. More interestingly, the sonication process during sample preparation for the TEM analysis did not cause nanoparticles to fall off the ECNFs, which signified the strong attachment between nanoparticles and

the ECNF surface. The perfectly crystalline structure of Co-CdSe nanoparticles was observed by high resolution-TEM (HR-TEM) (Figure 4d), recorded from the blue circled area of Figure 4c. As can be seen, the inner planar spacing of 0.367 nm, corresponding to the (111) crystallographic plane of CdSe (JCPDS: 65-2891), was clearly observed, revealing its excellent crystallinity. Furthermore, the heterojunction showed that the Co-CdSe nanoparticles attached to the surface of ECNFs had disordered stacking features, indicating its low crystallinity. Additionally, line EDS analysis of the sample was performed at randomly selected points on the line (Figure 5). As shown in the figure, C, Co, Cd, and Se were detected along the chosen line without any other elemental impurities. Hence, with these characterizations one can claim that the synthesized sample is purely made of C, Co, Cd, and Se, forming a ternary composite of Co-CdSe@ECNFs.

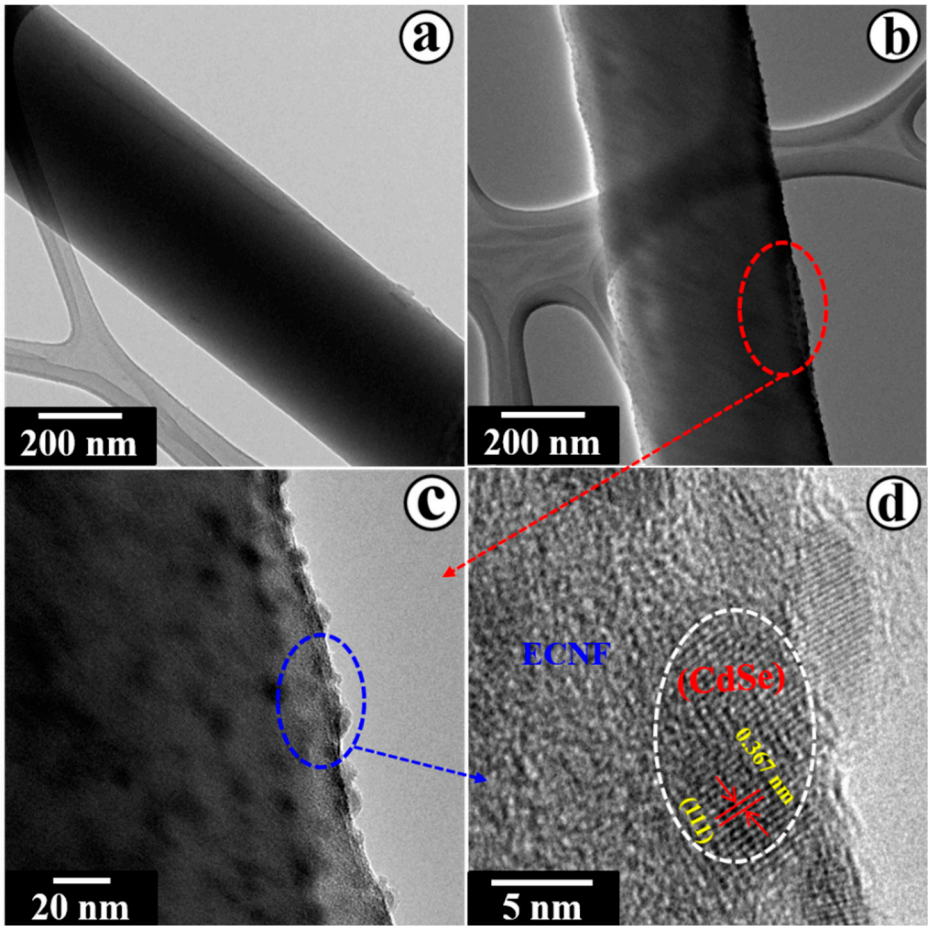

Figure 4. TEM images: (**a**) CNF, (**b**) Co-CdSe@ECNF, (**c**) magnified TEM image from the red circled area of (**b**), and (**d**) HR-TEM image from the blue circled area of (**c**).

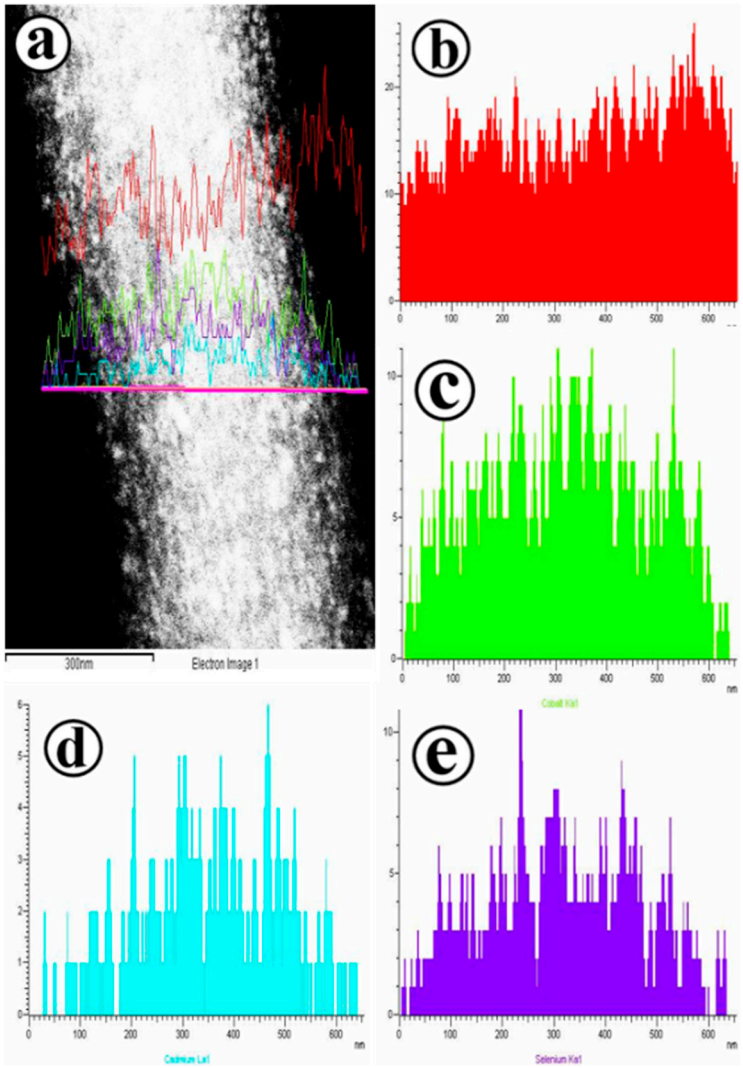

Figure 5. (**a**) Line TEM-EDS of Co-CdSe@ECNFs. Panels (**b**–**e**) represent line EDS spectra of carbon, cobalt, cadmium, and selenium, respectively.

The surface element compositions and chemical bonding states of Co-CdSe@ECNFs are presented in the X-ray photoelectron spectroscopy (XPS) results (Figure 6). The survey spectrum (Figure 6a) displays corresponding peaks of Co 2p, Cd 4d, Cd 3d, Cd 3p, Se 3d, Se 3s O 1s, and C 1s, indicating the formation of ternary composite. Figure 6b–e shows high-resolution spectra of Co 2p, Cd 3d, Se 3d, and C 1s, respectively. The peaks of Co 2p (Figure 6b) centered at 780.9 eV and 796.7 eV corresponding to Co $2p_{3/2}$ and Co $2p_{1/2}$, respectively, indicated the existence of Co as Co^{2+} [40]. Figure 6c shows a high-resolution spectrum of Cd 3d. The peaks located at 404.6 eV and 411.7 eV were attributed to the Cd $3d_{5/2}$ and Cd $3d_{3/2}$, respectively. This result confirms the presence of Cd^{2+} in Co-CdSe nanoparticles. The high-resolution spectrum of Se (Figure 6d) showed a peak centered at 54.2 eV, which was assigned to Se 3d [41]. The C 1s XPS spectrum of the sample is shown in Figure 6e. As shown in the figure, a characteristic peak obtained at 284.5 eV was attributed to C–C groups [42]. Thus, XPS analyses indicated the existence of Co^{2+} in CdSe crystal lattice forming a ternary composite of Co-CdSe@/ECNFs. In order to elucidate the stability of the photocatalyst, XPS analysis of the utilized sample (Co-CdSe@/ECNFs) was performed and the result is presented in the survey spectrum (Figure 6f) which displays corresponding peaks of the elements, matching those in Figure 6a. Since no significant change in the chemical composition of these elements was observed, the utilized sample retained its stability.

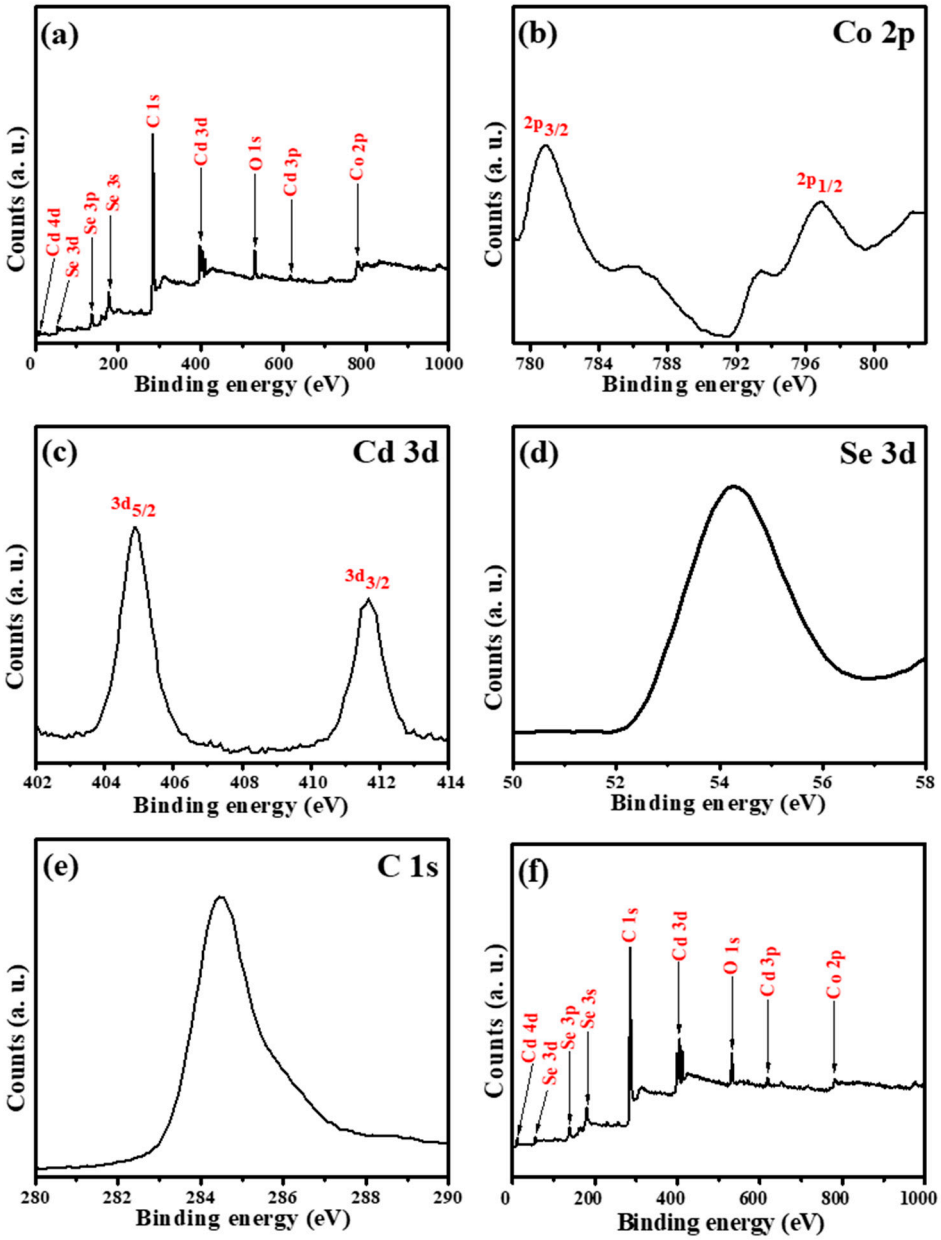

Figure 6. XPS spectra: (**a**) survey spectrum of Co-CdSe@ECNFs. Panels (**b**–**e**) represent the high-resolution spectra of Co 2p, Cd 3d, Se 3d, and C 1s, respectively, and (**f**) represents the survey spectrum of utilized Co-CdSe@ECNFs.

The degree of disorder as well as the composition of different samples are displayed in the Raman spectra in Figure 7. All the samples displayed corresponding peaks at 13,600 cm^{-1} for D band and 1586 cm^{-1} for G band. The D and G bands are associated with the sp^3 bonded carbon atoms in disordered carbonaceous matrix and the stretching of sp^2 bonded carbon atoms in graphitic carbon [43,44]. The magnified peaks displayed by the Co-CdSe@ECNFs sample at around 214 cm^{-1} and 413 cm^{-1} are assigned as the characteristic peaks of CdSe (inset). Thus, all the information derived from the Raman spectra confirms the formation of composite nanofibers.

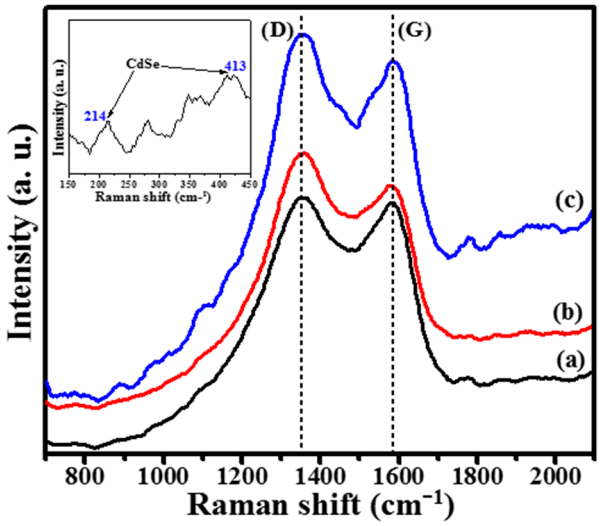

Figure 7. Raman spectra: (**a**) ECNFs, (**b**) CdSe@ECNFs, and (**c**) Co-CdSe@ECNFs. Inset: magnified peaks of CdSe. (D: D band and G: G band).

Investigation of the photocatalytic activity of a photocatalyst depends upon its light absorption behavior, which plays an important role in determining whether the photocatalyst works under visible light or UV-light. In order to determine this crucial factor UV-Vis diffusive reflectance spectra (DRS) of different samples were measured, and the results are plotted in Figure 8. As shown in Figure 8, ECNFs present the absorption band in visible light and UV-light regions. Meanwhile, it was observed that ECNFs loaded with undoped/Co-doped CdSe nanoparticles displayed obvious visible light absorption behavior, signifying their ability to harvest visible light.

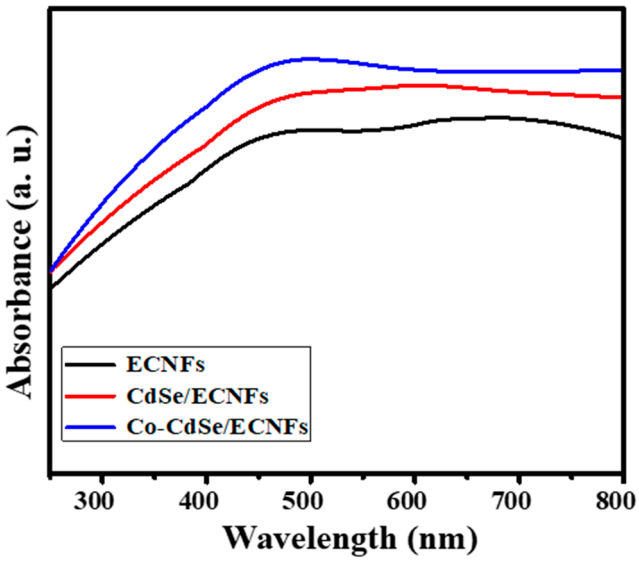

Figure 8. UV-Vis diffusive reflectance spectra.

The photocatalytic performances of Co-CdSe@ECNFs and CdSe@ECNFs towards the photodegradation of methylene blue (MB) and rhodamine B (RhB) were evaluated under visible light irradiation. Figure 9a,b shows degradation curves of MB and RhB solutions utilizing different samples along with blank tests. The degradation is represented as the variation of (C_t/C_o) with irradiation time, where C_o is the initial concentration and C_t is the remaining concentration of the dye solutions at time t. As illustrated in the figures, the blank tests showed negligible degradation of both dye solutions. Similarly, negligible degradation/absorbance of both dye solutions was observed when

utilizing ECNFs alone. In contrast, Co-CdSe@ECNFs degraded more than 90% of MB within 70 min, while CdSe@ECNFs degraded only 85% of MB within this time. Additionally, the photocatalytic performance of Co-CdSe@ECNFs compared to CdSe@ECNFs for RhB degradation was found to be higher. More than 87% of RhB was degraded within 90 min when utilizing Co-CdSe@ECNFs, but only 81% of RhB was degraded within this time when CdSe@ECNFs was utilized under similar conditions. Based on these results, Co-CdSe@ECNFs was found to be a superior photocatalyst to CdSe@ECNFs for dye degradation under visible light irradiation. The absorbance variation of MB and RhB solutions utilizing Co-CdSe@ECNFs under visible light irradiation at different time intervals is shown in Figure 9c,d. As can be seen, with the increase in irradiation time, all the corresponding absorbance peaks of MB and RhB solutions located at 665 nm and 554 nm were observed to gradually diminish. Furthermore, the color of the corresponding dye solutions gradually weakened with time in the presence of Co-CdSe@ECNFs (insets, Figure 9c,d).

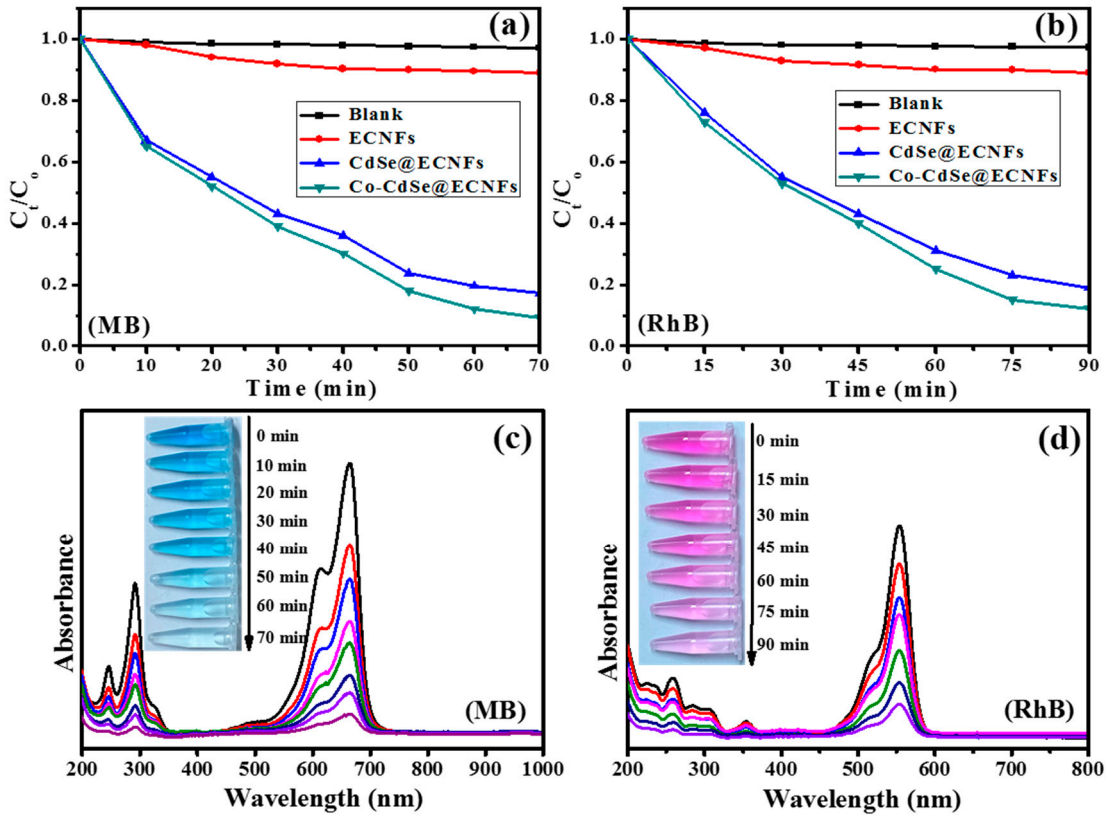

Figure 9. Photocatalytic performance of ECNFs, CdSe@ECNFs, and Co-CdSe@ECNFs towards the photodegradation of (**a**) methylene blue (MB) and (**b**) rhodamine B (RhB) solutions. The absorbance variation of (**c**) MB and (**d**) RhB solutions utilizing Co-CdSe@ECNFs. Insets: digital photographs showing gradual change in the color of corresponding dye solution with irradiation time.

Besides photocatalytic efficiency, the stability of the photocatalyst is another important aspect for practical application. Therefore, cycling experiments for MB and RhB degradation utilizing Co-CdSe@ECNFs were conducted under visible light irradiation. For cycling experiments, the used sample was centrifuged and dried at room temperature. Based on the results (Figure 10a,b), the photocatalytic performance of Co-CdSe@ECNFs was found to be stable up to the third cycle, but there was a slight decrease in activity during cycling experiments, which could be due to the loss of photocatalyst during the separation process. The reaction kinetics of MB and

RhB photodegradation utilizing Co-CdSe@ECNFs and CdSe@ECNFs were calculated with the Langmuir–Hinshelwood equation.

$$r = -\frac{dc}{dt} = \frac{k_r KC}{1 + KC} \quad (1)$$

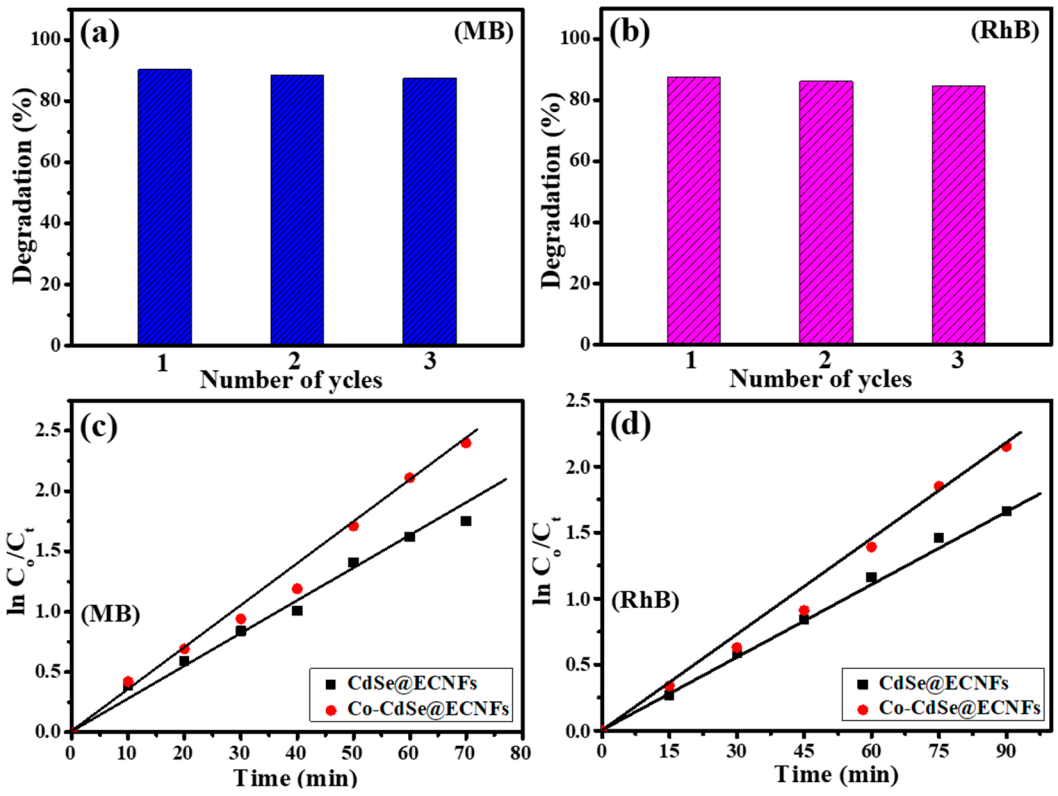

Figure 10. Cycling experiments of the photodegradation of (**a**) MB and (**b**) RhB solutions utilizing Co-CdSe@ECNFs. Photodegradation kinetics of (**c**) MB and (**d**) RhB solutions over different photocatalysts under visible light irradiation.

As the initial concentration of MB and RhB solutions were very low (C_o = 10 mg/L), Equation (1) was reduced to a pseudo-first-order kinetics equation [45] as:

$$ln\ C_o/C_t = k_{app}t \quad (2)$$

Here, C_o, C_t, and k_{app} represent the initial concentration, concentration at time t (min), and apparent rate constant (min^{-1}), respectively. The k_{app} is determined by plotting the graph of $ln(C_o/C_t)$ vs. reaction time. The photodegradation kinetics of MB and RhB were calculated using Equation (2), and results are presented in Figure 10c,d. The linear relationship of $ln(C_o/C)$ vs. reaction time could suggest the pseudo-first-order kinetics of the photodegradation reaction. The apparent rate constants of MB and RhB degradation over Co-CdSe@ECNFs were determined to be 0.035 min^{-1} and 0.022 min^{-1}, respectively. Likewise, the apparent rate constants of MB and RhB degradation over CdSe@ECNFs were determined to be 0.028 min^{-1} and 0.018 min^{-1} respectively. Thus, the above results signify the role of Co^{2+} as a dopant for enhancing the photocatalytic activity of Co-CdSe@ECNFs under visible light irradiation.

The possible mechanism scheme for enhanced photocatalytic activity of Co-CdSe@ECNFs is shown in Figure 11. When Co-CdSe@ECNFs photocatalyst was irradiated with visible light, electrons (e^-) from the valence band (VB) of Co-CdSe were excited to the conduction band (CB), leaving behind holes (h^+). Some of the excited electrons in CB reacted directly with dissolved oxygen to

generate reactive oxygen species (ROS), that is, oxygen peroxide radicals ($O_2^{\bullet-}$), because of the more negative E_{CB} of Co-CdSe than $O_2/O_2^{\bullet-}$ potential (−0.33 eV versus normal hydrogen electrode (NHE)), while other electrons transferred to the ECNFs due to their good electrical conductivity and close attachment with Co-CdSe nanoparticles. Transferred electrons also reacted with oxygen to generate $O_2^{\bullet-}$. Additionally, doped Co^{2+} could play an important role in capturing and transferring electrons to prevent the recombination of photogenerated charge carriers [46]. Thus, ROS produced during the reaction process are responsible for the photodegradation of MB dye and RhB [47]. Conversely, photogenerated holes in the VB of Co-CdSe could not react with water to generate hydroxyl radicals ($OH^{\bullet}$) as the E_{VB} was more negative than the $OH^{\bullet}/OH^-$ potential (2.38 eV versus an NHE) [48]. As a consequence, holes were involved in the reduction reaction directly.

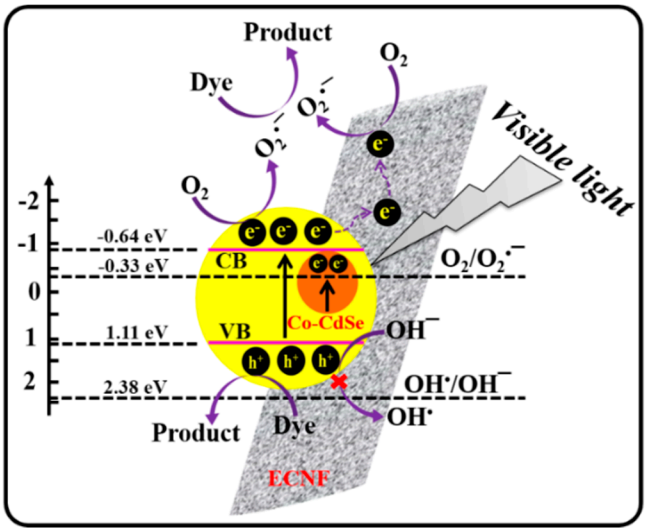

Figure 11. Schematic illustration for the photodegradation of dye solution using proposed Co-CdSe@ECNFs.

$$\text{Dye} + O_2^{\bullet-} \rightarrow CO_2 + H_2O + \text{mineralized products}$$

3. Materials and Methods

3.1. Materials

Polyacrylonitrile (PAN, MW-150000), cobalt acetate tetrahydrate ($Co(CH_3COO)_2{\cdot}4H_2O$), cadmium acetate dihydrate ($Cd(CH_3COO)_2{\cdot}2H_2O$), selenium powder (Se), methylene blue (MB), and rhodamine B (RhB) were purchased from Sigma-Aldrich, St. Louis, MO, USA. *N,N*-dimethylformamide (DMF) was purchased from SAMCHUN PURE CHEMICAL, (Mogok-dong) 117, Gyeonggi-d, South Korea. All the chemicals were used as received without further purification.

3.2. Fabrication of Ternary Composite of Co-CdSe@ECNFs

Ternary composite of Co-CdSe@ECNFs was prepared by electrospinning followed by carbonization. For the fabrication of Co^{2+}/Cd^{2+}/Se PAN precursor nanofibers, first, 1 mmol of Se powder was dispersed in 12 g of DMF, then 1 mmol of cobalt acetate and 1 mmol of cadmium acetate were added to the above solution with strong magnetic stirring for 1 h. Finally, 1 g of PAN was added to the mixture solution and left for 12 h of continuous magnetic stirring in order to obtain a homogeneous solution. The final solution was loaded into a 5 mL injection syringe provided with a plastic micro-tip, and electrospinning of the precursor solution was carried out using a high voltage power supply at an applied voltage of 18 kV. In this process, the distance between the tip and collector was kept at 12 cm, while the developing electrospun nanofibers were collected on a drum collector which was rotated at a constant speed by a DC motor. All the experimental works were conducted at room temperature and

atmospheric pressure. The electrospun nanofibers were vacuum dried at 70 °C for 12 h to remove the residual solvent. For carbonization, vacuum-dried electrospun precursor nanofibers were stabilized at 250 °C for 2 h with a heating rate of 1 °C/min and cooled to room temperature, they were then carbonized in Ar atmosphere at 800 °C for 2 h with a heating rate of 5 °C/min. After cooling to room temperature, ternary composite of Co-CdSe@ECNFs was obtained. For comparison, composite of CdSe@ECNFs was prepared under similar conditions without adding Co^{2+}.

3.3. Characterization

The crystalline phase of samples was investigated by an X-ray diffractometer (XRD, Empyrean, PANAlytical, Eindhoven 5651 GH, Netherlands) with Cu Kα (λ = 1.540 Å) radiation over Bragg angles ranging from 10° to 70°. Field-emission scanning electron microscopy (FESEM, GeminiSEM 500, Carl Zeiss Microscopy GmbH, 73447 Oberkochen, Germany) equipped with energy-dispersive X-ray spectroscopy (EDS) was used to study the morphology and to analyze the elemental composition of the samples. Transmission electron microscopy was applied to study the morphology and distribution of nanoparticles on ECNFs. Additionally, high-resolution images (HR-TEM) of the prepared sample were observed using a transmission electron microscope (TEM, JEM-2200FS, JEOL Ltd., Akishima, Tokyo, Japan) equipped with EDS. The surface element composition analysis of Co-CdSe@ECNFs was recorded using X-ray photoelectron spectroscopy (XPS, AXIS-NOVA, Kratos Analytical Ltd., Manchester, M17 1GP, UK). Raman spectroscopy was utilized to determine the degree of disorder and the composition of the samples using a micro-Raman spectrometer (Tokyo instrument, Nanofinder 30, Tokyo, Japan). UV-Vis diffusive reflectance spectra (DSR) of composites were measured using a UV-Vis spectrophotometer (UV-2600 240 EN, SHIMADZU CORPORATION, Kyoto, Japan).

3.4. Photocatalytic Activity Investigation

Photocatalytic activities of CdSe@ECNFs and Co-CdSe@ECNFs were investigated by observing the degradation of MB and RhB dye solutions using a solar simulator with an internal xenon lamp (DYX300P, DYE TECH Co., Seoul, Korea) equipped with a UV cut-off filter. In this experiment, 50 mL of dye solution, with an initial concentration of 10 mg L^{-1} was mixed with 50 mg of photocatalyst in a glass vial and magnetically stirred for 30 min under dark conditions in order to establish an adsorption/desorption equilibrium between dye molecules and photocatalysts. After that, visible light (λ > 420 nm) obtained from a 200 W xenon lamp was irradiated under constant magnetic stirring. In order to investigate the self-degradation of dye solutions under identical conditions, blank tests were performed without utilizing photocatalyst. Aliquots were taken at regular time intervals and the concentration of the dye solution was measured spectrophotometrically by recording the absorbance using a UV-Vis spectrophotometer (HP 8453 UV-Vis spectroscopy system, Hudson, MA, USA).

4. Conclusions

This research aimed to present a successful effort towards fabricating a ternary composite with inorganic–organic heterostructure composed of in-situ-synthesized Co-CdSe nanoparticles and ECNFs using electrospinning followed by carbonization. All the samples were characterized using FESEM, XRD, TEM, XPS, Raman spectroscopy, and UV-Vis spectroscopy. Thus, the obtained ternary composites (Co-CdSe@ECNFs) showed enhanced photocatalytic activity towards the photodegradation of MB and RhB under visible light due to sufficient electron–hole separation ability, compared to that of CdSe@ECNFs. Similarly, a large length-to-diameter ratio of ECNFs could make the separation process of photocatalyst simpler after use. Finally, the impact of Co doping on the photocatalytic activity of ternary composite has been reported.

Author Contributions: For this research article, the individual contribution of authors was as follows: conceptualization and data analysis, G.P. and K.R.G.; methodology, G.P., O.H.K., Y.W.P., and Y.-S.K.; manuscript preparation, G.P. and K.R.G.; writing—review and editing, G.P. and M.P.; resources and supervision, M.P.; funding acquisition, M.P. All authors have read and agreed to the published version of the manuscript.

Funding: This research was supported by the Traditional Culture Convergence Research Program through the National Research Foundation of Korea (NRF) funded by the Ministry of Science, CT & Future Planning (2018M3C1B5052283) and National Research Foundation of Korea (NRF) grant funded by the Korea Government (MSIT) (No.NRF-2019R1A2C1004467).

Conflicts of Interest: The authors declare no conflicts of interest.

References

1. Correia, V.M.; Stephenson, T.; Judd, S.J. Characterization of textile waste water-A review. *Environ. Technol.* **1994**, *15*, 917. [CrossRef]
2. Wang, J.L.; Xu, L.J. Advanced oxidation process for wastewater treatment: Formation of hydroxyl radical and application. *Crit. Rev. Environ. Sci. Technol.* **2012**, *42*, 251–325. [CrossRef]
3. Sharma, P.; Kaur, H.; Sharma, M.; Sahore, V. A review on applicability of naturally available adsorbent for the removal of hazardous dyes from aqueous waste. *Environ. Monit. Assess.* **2011**, *183*, 151–195. [CrossRef] [PubMed]
4. Hoffmann, M.R.; Martin, S.T.; Choi, W.; Bahnemannt, D.W. Environmental Applications of Semiconductor Photocatalysis. *Chem. Rev.* **1995**, *95*, 69–96. [CrossRef]
5. Mohamed, H.H.; Bahnemann, D.W. The role of electron transfer in photocatalysis: Fact and fictions. *Appl. Catal. B* **2012**, *128*, 91–104. [CrossRef]
6. Sapkota, K.P.; Lee, I.; Hnif, M.A.; Islam, M.A.; Akter, J.; Hahn, J.R. Enhanced Visible-Light Photocatalysis of Nanocomposites of Copper Oxide and Single-Walled Carbon Nanotubes for the Degradation of Methylene Blue. *Catalysts* **2020**, *10*, 297. [CrossRef]
7. Bahnemann, D.; Henglein, A.; Lilie, J.; Spanhel, L. Flash photolysis observation of the absorption spectra of trapped positive holes and electrons in colloidal titanium dioxide. *J. Phys. Chem.* **1984**, *88*, 709–711. [CrossRef]
8. Manjoor, T.; Pandith, A.H. Enhancing the photoresponse by CdSe-Dye-TiO_2-based multijunction systems for efficient dye-sensitized solar cells: A theoretical outlook. *J. Comput. Chem.* **2019**, *40*, 2444–2452. [CrossRef]
9. Fujishima, A.; Honda, K. Electrochemical photolysis of water at a semiconductor electrode. *Nature* **1972**, *238*, 37–38. [CrossRef]
10. Livraghi, S.; Paganini, M.C.; Giamello, E.; Selloni, A.; Valentin, C.D.; Pacchioni, G. Origin of photoactivity of nitrogen-doped titanium dioxide under visible light. *J. Am. Chem. Soc.* **2006**, *128*, 15666–15671. [CrossRef]
11. Yu, J.G.; Yu, X.X.; Huang, B.B.; Zhang, X.Y.; Dai, Y. Hydrothermal synthesis and visible-light photocatalytic activity of novel cage-like ferric oxide hollow spheres. *Cryst. Growth Des.* **2009**, *9*, 1474–1480. [CrossRef]
12. Li, Q.; Guo, B.; Yu, J.; Ran, J.; Zhang, B.; Yan, H.; Gong, J.R. Highly efficient visible-light-driven photocatalytic hydrogen production of CdS-cluster-decorated graphene nanosheets. *J. Am. Chem. Soc.* **2011**, *133*, 10878–10884. [CrossRef]
13. Panthi, G.; Yousef, A.; Barakat, N.A.M.; Khalil, K.A.; Akhter, S.; Choi, Y.; Kim, H.Y. Mn_2O_3/TiO_2 nanofibers with broad-spectrum antibiotics effect and photocatalytic activity for preliminary stage of water desalination. *Ceram. Int.* **2013**, *39*, 2239–2246. [CrossRef]
14. Meng, X.G.; Liu, L.Q.; Ouyang, S.X.; Xu, H.; Wang, D.F.; Zhao, N.Q.; Ye, J.H. Nanometals for Solar-to-Chemical Energy Conversion: From Semiconductor-Based Photocatalysis to Plasmon-Mediated Photocatalysis and Photo-Thermocatalysis. *Adv. Mater.* **2016**, *28*, 6781–6803. [CrossRef] [PubMed]
15. Lang, X.J.; Chen, X.D.; Zhao, J.C. Heterogeneous visible light photocatalysis for selective organic transformations. *Chem. Soc. Rev.* **2014**, *43*, 473–486. [CrossRef] [PubMed]
16. Kisch, H. Semiconductor Photocatalysis-Mechanistic and Synthetic Aspects. *Angew. Chem. Int. Ed.* **2013**, *52*, 812–847. [CrossRef] [PubMed]
17. Joa, W.K.; Selvam, N.C.S. Synthesis of GO supported Fe_2O_3-TiO_2 nanocomposites for enhanced visible-light photocatalytic applications. *Dalton Trans.* **2015**, *44*, 16024–16035. [CrossRef] [PubMed]
18. Lee, A.; Joseph, A.; Libera, J.A.; Waldman, R.Z.; Ahmed, A.; Avila, J.R.; Elam, J.W.; Darling, S.B. Conformal Nitrogen-Doped TiO_2 Photocatalytic Coatings or Sunlight-Activated Membranes. *Sustain. Syst.* **2017**, *1*, 1600041. [CrossRef]
19. Paola, A.D.; García-López, E.; Marcì, G.; Palmisano, L. A survey of photocatalytic materials for environmental remediation. *J. Hazard. Mater.* **2012**, *211–212*, 3–29. [CrossRef]

20. Peng, P.; Milliron, D.J.; Hughes, S.M.; Johnson, J.C.; Alivisatos, A.P.; Saykally, R.J. Femtosecond Sepectroscopy of Carrier Relaxation Dynamics in Type II CdSe/CdTe Tetrapod Heteronanostructures. *Nano Lett.* **2005**, *5*, 1809–1813. [CrossRef]
21. Tsui, E.Y.; Hartstein, K.H.; Gamelin, D.R. Selenium Redox Reactivity on Colloidal CdSe Quantum Dot Surfaces. *J. Am. Chem. Soc.* **2016**, *138*, 11105–11108. [CrossRef] [PubMed]
22. Wang, P.; Li, D.Z.; Chen, J.; Zhang, X.Y.; Xian, J.J.; Yang, X.; Zheng, X.Z.; Li, X.F.; Shao, Y. A novel and green method to synthesize CdSe quantum dots-modified TiO_2 and its enhanced visible light photocatalytic activity. *Appl. Catal. B* **2014**, *160*, 217–226. [CrossRef]
23. Yang, X.; Zhang, W.; Zhao, Z.; Li, N.; Mou, Z.; Sun, D.; Cai, Y.; Wang, W.; Lin, Y. Quercertin loading CdSe/ZnS nanoparticles as efficient antibacterial and anticancer materials. *J. Inorg. Biochem.* **2017**, *167*, 36–48. [CrossRef] [PubMed]
24. Ullah, K.; Kim, Y.-H.; Lee, B.-E.; Jo, S.-B.; Zhu, L.; Ye, S. Visible light induced catalytic properties of CdSe-graphene nanocomposites and study its bactericidal effect. *Chin. Chem. Lett.* **2014**, *25*, 941–946. [CrossRef]
25. Lin, Y.; Wu, S.H.; Li, X.; Wu, X.; Yang, C.P.; Zeng, G.M.; Peng, Y.R.; Zhou, Q.; Lu, L. Microstructure and performance of Z-scheme photocatalyst of silverphosphate modified by MWCNTs and Cr-doped $SrTiO_3$for malachite green degradation. *Appl. Catal. B* **2018**, *227*, 557–570. [CrossRef]
26. Yang, Y.; Kao, L.C.; Liu, Y.Y.; Sun, K.; Yu, H.T.; Guo, J.H.; Liou, S.Y.H.; Hoffmann, M.R. Cobalt-Doped Black TiO_2 Nanotube Array as a Stable Anode for Oxygen Evolution and Electrochemical Wastewater Treatment. *ACS Catal.* **2018**, *8*, 4278–4287. [CrossRef]
27. Wang, W.S.; Ye, Y.F.; Feng, J.; Chi, M.F.; Guo, J.H.; Yin, Y.D. Enhanced Photoreversible Color Switching of Redox Dyes Catalyzed by Barium-Doped TiO_2 Nanocrystals. *Angew. Chem. Int. Ed.* **2015**, *54*, 1321–1326. [CrossRef]
28. Ma, C.C.; Zhou, M.J.; Wu, D.; Feng, M.Y.; Liu, X.L.; Huo, P.W.; Shi, W.D.; Ma, Z.F.; Yan, Y.S. One-step hydrothermal synthesis of cobalt and potassium codoped CdSe quantum dots with high visible light photocatalytic activity. *CrystEngComm* **2015**, *17*, 1701–1709. [CrossRef]
29. Nishikiori, H.; Sato, T.; Kubota, S.; Tanaka, N.; Shimizu, Y.; Fujii, T. Preparation of Cu-doped TiO_2 via refluxing of alkoxide solution and its photocatalytic properties. *Res. Chem. Intermed.* **2012**, *38*, 595–613. [CrossRef]
30. Veeramani, V.; Chen, Y.-H.; Wang, H.-C.; Hung, T.-F.; Chang, W.-S.; Wei, D.-H.; Hu, S.-F.; Liu, R.-S. CdSe/ZnS QD@CNT nanocomposite photocathode for improvement on charge overpotential in photoelectrochemical Li-O_2 batteries. *Chem. Eng. J.* **2018**, *349*, 235–240. [CrossRef]
31. Payan, A.; Fattahi, M.; Jorfi, S.; Roozbehani, B.; Payan, S. Synthesis and characterization of titanate nanotube/single-walled carbon nanotube (TNT/SWCNT) porous nanocomposite and its photocatalytic activity on 4-chlorophenol degradation under UV and solar irradiation. *Appl. Surf. Sci.* **2018**, *434*, 336–350. [CrossRef]
32. Zhou, M.J.; Li, J.Z.; Ye, Z.F.; Ma, C.C.; Wang, H.Q.; Huo, P.W.; Shi, W.D.; Yan, Y.S. Transfer Charge and Energy of Ag@CdSe QDs-rGO Core-Shell Plasmonic Photocatalyst for Enhanced Visible Light Photocatalytic Activity. *ACS Appl. Mater. Interfaces* **2015**, *7*, 28231–28243. [CrossRef]
33. Cung, D.; Nguyen, T.; Zhu, L.; Zhang, Q.; Cho, K.Y.; Oh, W.-C. A new synergetic mesoporous silica combined to CdSe-graphene nanocomposite for dye degradation and hydrogen evolution in visible light. *Mater. Res. Bull.* **2018**, *107*, 14–27.
34. Ng, Y.H.; Ikeda, S.; Harada, T.; Higashida, S.; Sakata, T.; Mori, H.; Matsumura, M. Fabrication of Hollow Carbon Nanospheres Encapsulating Platinum Nanoparticles Using a Photocatalytic Reaction. *Adv. Mater.* **2007**, *19*, 597–601. [CrossRef]
35. Zhao, X.H.; Su, S.; Wu, G.L.; Li, C.Z.; Qin, Z.; Lou, X.D.; Zhou, J.G. Facile synthesis of the flower-like ternary heterostructure of Ag/ZnO encapsulating carbon spheres with enhanced photocatalytic performance. *Appl. Surf. Sci.* **2017**, *406*, 254–264. [CrossRef]
36. Mu, J.; Shao, C.; Guo, Z.; Zhang, M.; Zhang, Z.; Zhang, P.; Chen, B.; Liu, Y. In_2O_3 nanocubes/carbon nanofibers heterostructures with high visible light photocatalytic activity. *J. Mater. Chem.* **2012**, *22*, 1786–1793. [CrossRef]
37. Bonino, C.A.; Ji, L.; Lin, Z.; Toprakci, O.; Zhang, X.; Khan, S.A. Electrospun Carbon-Tin Oxide Composite Nanofibers for Use as Lithium Ion Battery anodes. *ACS Appl. Mater. Interfaces* **2011**, *3*, 2534–2542. [CrossRef]

38. Lee, J.S.; Kwon, O.S.; Park, S.J.; Park, E.Y.; You, S.A.; Yoon, H.; Jang, J. Fabrication of Ultrafine Metal-Oxide-Decorated Carbon Nanofibers for DMMP Sensor Application. *ACS Nano* **2011**, *5*, 7992–8001. [CrossRef]
39. Mao, Z.; Lin, H.; Xu, M.; Miao, J.; He, S.J.; Li, Q. Fabrication of co-doped CdSe quantum dot-sensitized TiO_2 nanotubes by ultrasound-assisted method and their photoelectrochemical properties. *J. Appl. Electrochem.* **2018**, *48*, 147–155. [CrossRef]
40. Li, J.; Peng, Y.; Qian, X.H.; Lin, J. Few-layer Co-doped MoS_2 nanosheets with rich active sites as an efficient cocatalyst for photocatalytic H_2 production over CdS. *Appl. Surf. Sci.* **2018**, *452*, 437–442. [CrossRef]
41. Tang, C.; Pu, Z.; Liu, Q.; Asiri, A.M.; Sun, X.; Luo, Y.; He, Y. In Situ Growth of NiSe Nanowire Film on Nickel Foam as an Electrode for High-Performance Supercapacitors. *ChemElectroChem* **2016**, *2*, 1903–1907. [CrossRef]
42. An, G.-H.; Ahn, H.-J. Surface modification of RuO_2 nanoparticles-carbon nanofiber composites for electrochemical capacitors. *J. Electroanal. Chem.* **2015**, *744*, 32–36. [CrossRef]
43. Yang, J.; Zhang, Y.; Kim, D.Y. Electrochemical sensing performance of nanodiamond-derived carbon nano-onions: Comparison with multiwalled carbon nanotubes, graphite nanoflakes, and glassy carbon. *Carbon* **2016**, *98*, 74–82. [CrossRef]
44. Fan, G.; Ge, J.; Kim, H.Y.; Ding, B.; Al-Deyab, S.S.; El-Newehy, M.; Yu, J. Hierarchical porous carbon nanofibrous membranes with an enhanced shape memory property for effective adsorption of proteins. *RSC Adv.* **2015**, *5*, 64318–64325. [CrossRef]
45. Zhang, Z.; Shao, C.; Li, X.; Wang, C.; Zhang, M.; Liu, Y. Electrospun Nanofibers of *p*-Type NiO/*n*-Type ZnO Heterojunctions with Enhanced Photocatalytic Activity. *ACS Appl. Mater. Interfaces* **2010**, *2*, 2915–2923. [CrossRef]
46. Ma, C.; Liu, X.; Zhou, M.; Feng, M.; Wu, Y.; Huo, P.; Pan, J.; Shi, W.; Yan, Y. Metal ion doped CdSe quantum dots prepared by hydrothermal synthesis: Enhanced photocatalytic activity and stability under visible light. *Desalin. Water. Treat.* **2015**, *56*, 2896–2905. [CrossRef]
47. Makhluf, S.; Dror, R.; Nitzan, Y.; Abramovich, Y.; Jelinek, R.; Gedanken, A. Microwave-assisted synthesis of nanocrystalline MgO and its use as a bacteriocide. *Adv. Funct. Mater.* **2005**, *15*, 1708–1715. [CrossRef]
48. Li, W.; Wang, G.J.; Feng, Y.M.; Li, Z.C. Efficient photocatalytic performance enhancement in Co-doped ZnO nanowires coupled with CuS nanoparticles. *Appl. Surf. Sci.* **2018**, *428*, 154–164. [CrossRef]